geosciences

MDPI

Article

Geomorphology of the Coastal Sand Dune Fields and Their Association with the Palaeolandscape Evolution of Akrotiri Peninsula, Lemesos, Cyprus

Miltiadis Polidorou * and Niki Evelpidou

Faculty of Geology & Geoenvironment, National & Kapodistrian University of Athens, Panepistimioupolis Zografou, 157 84 Athens, Greece; evelpidou@geol.uoa.gr
* Correspondence: mpolidorou@geol.uoa.gr

Abstract: Two well-developed late Pleistocene dune fields have been identified on the western and eastern side of Akrotiri promontory (Lemesos, Cyprus). The dune fields extend immediately from the low level of their source beaches onto higher ground (>48 m amsl). Geomorphic observations supported by OSL dating and sedimentological data provided evidence of the dune development and for the palaeogeographic reconstruction of the area. Relative sea level changes and wave action during the upper Pleistocene and Holocene played an important role into the development of the palaeolandscape and affected the formation of the dunes. From the collected data the development of the western dune field started at 56.2 ± 5.5 ka when the relative sea level was at approximately −60 m and contributed to the development of the western tombolo of the area whereas the eastern dune field developed in the late Holocene, after the formation of the eastern spit that resulted in the formation of the Akrotiri Salt lake.

Keywords: Cyprus; luminescence dating; aeolian deposits; coastal evolution; Pleistocene; Holocene

check for updates

Citation: Polidorou, M.; Evelpidou, N. Geomorphology of the Coastal Sand Dune Fields and Their Association with the Palaeolandscape Evolution of Akrotiri Peninsula, Lemesos, Cyprus. *Geosciences* **2021**, *11*, 448. https://doi.org/10.3390/geosciences11110448

Academic Editors: Maša Surić, Lara Wacha and Jesus Martinez-Frias

Received: 13 October 2021
Accepted: 28 October 2021
Published: 30 October 2021

Publisher's Note: MDPI stays neutral with regard to jurisdictional claims in published maps and institutional affiliations.

Copyright: © 2021 by the authors. Licensee MDPI, Basel, Switzerland. This article is an open access article distributed under the terms and conditions of the Creative Commons Attribution (CC BY) license (https://creativecommons.org/licenses/by/4.0/).

1. Introduction

Dune systems are important geomorphological features found along a significant part of the world's coastline. An interaction of natural factors such as sediment supply, flat topography, strong sand-moving winds and vegetation cover are responsible for the accumulation and formation of sand dunes [1–8]. Storms and sea level fluctuations can also impact dune system development and mobility, through changes in sediment supply and vegetation [9,10].

Sediment supply from the coast is the source for the formation and growth of coastal sand dunes [11]. Change in sediment supply can modify dune mobility. Specifically, high sand supply can bury vegetation, resulting in drifting sand and mobile sand dunes, while low sand input can encourage vegetation survival, leading to an increase in dune stability [12].

At the most basic level, sand dunes can be categorized in those that form from the direct supply of sediment from the beach face (primary dunes), and those that form from the subsequent modification of primary dunes (secondary dunes). Primary dunes are composed of sand, blown directly from the beach face (active beach), whereas secondary dunes develop following the subsequent modification of primary dunes. Primary dunes are those closest to the shoreline, dynamically linked to beach processes and significantly influenced by wave action [13–15].

Vegetation is a crucial element in the evolution of dune landscapes. It is necessary to trap the sand for dunes to grow but also to stabilize the ground. The pioneer species, by this action, will facilitate the establishment of other species, increasing biodiversity (flora and fauna) [10]. The main driver for coastal sand dune erosion is the near-surface wind vector (speed, direction) consistent with standard formulations of aeolian sediment

transport models [16,17]. Wind velocity is generally reduced by plant cover, encouraging deposition and trapping of wind-borne sand. However, wind velocity may also accelerate locally in gaps between plants, especially those having a clumpy form.

Reconstructing coastal evolution is typically based on geological evidence derived from field observations and sedimentary or paleontological laboratory analyses, but receives critical support from geochronology information obtained by numeric dating methods [18,19]. OSL dating of quartz using the single-aliquot regenerative-dose protocol (SAR) [20] was successfully applied in many of studies to Holocene coastal sand dunes [21,22] and inland dunes [23–25].

Very few studies have focused on geomorphological evolution and palaeogeography of coastal dunes in Cyprus. The majority of the studies were focused on the flora and fauna development on the dune formations without emphasizing to the geomorphological and palaeogeographical evolution [26–28]. In this context, the aim of this study is to investigate the dunes of the southern coast of Cyprus and furthermore to evaluate the usability of sand dune systems as a tool for the palaeogeographic reconstruction of similar settings in the area of the Eastern Mediterranean.

1.1. Study Area

Akrotiri Peninsula is the southernmost part of the island of Cyprus. It is located approximately 5 km to the southwest of the port of Lemesos. 90% of the peninsula is situated within the British Sovereign Base Area. Akrotiri Peninsula covers roughly 60 km^2 (Figure 1). It includes a southern plateau formed by uplifted marine terraces [29–31] with a maximum elevation of over 60 m amsl. The northern part lies in general below 10 m elevation, covered by alluvial fan deposits which are the result of the continuous supply of material by the Kouris river. The Akrotiri aquifer consist the most important porous aquifer of Southern Cyprus. The southern boundary of the aquifer runs along the edge of the Akrotiri salt lake. The Akrotiri aquifer has an approximate surface area of 45 km^2 and consists of deltaic sediments, deposited in two big fan deltas, coming from the Kouris River in the west. The Kouris River is the largest river in Cyprus and drains a catchment area of 300 km^2, extending far up into the Troodos mountains [32]. Its middle is occupied by the Akrotiri Salt Lake which is covering an area of approximately 20 km^2. Today, the maximum depth of the Salt Lake reaches 2.8 m below mean sea level during the winter period [30,31,33]. The northern and southern part of the peninsula is connected by two tombolos. The western tombolo consists mainly of sands and gravels and its formation is connected with the material discharged by Kouris river [30,31]. The eastern tombolo consists mainly of sand and it is formed by the eroded material (western dune field sand and exposed sandy marls) of the western part of the peninsula, which follows the anticlockwise long shore drift [34] and the western prevailing winds of the study area [30,31].

1.2. Climate

The Eastern Mediterranean basin is located on the leeward side of the Asia Minor peninsula, where a cyclonic atmospheric circulation predominates [35–37]. This cyclogenetic activity generates a counter-clockwise circulation, initially passing through the Aegean Sea and then blowing over the Levantine Basin [38,39]. Winds are predominantly from the southwest-to-north and occasionally from the north-to-east during winter. During spring, winds are from the west-to-north, whereas they are from northwest to west during the summer and autumn. Crucially, north- westerly to southwesterly wind flows are particularly felt during storm events. Similar westerly and southwesterly cyclonic winter storm winds in Israel enable sand-transport [40–42]. These storms, which provide most of the annual rainfall, are usually not a constraint on sand transport, as rapid surface evaporation by the winds makes the upper sand surface erodible in minutes following rainfall [43].

Climatic data were obtained for the period 1982 to 2018 (Cyprus Department of Meteorology). The annual main wind direction is West 22% to West South West 16%. Main

wind directions for a period of one year are presented in Figure 2 which include mainly W to SSW winds for the major part of the year (approx. 80%) and periodically E to ENE winds (approx. 20%). The annual mean precipitation of the study area is 377 mm. The average wind velocity for the study area is 14.05 km/h for a period of 36 years. The maximum annual average wind speed was 15.3 km/h in 2016 and the minimum 11.5 km/h in 2007. July has the highest average wind velocity with 15.8 km/h, while October has the lowest average wind velocity with 10.6 km/h. The palaeoclimatic conditions according to Schilman et al., (2001) [44], seem to follow the general aridification trend which has begun about 7000 years ago in the eastern Mediterranean region [44–46].

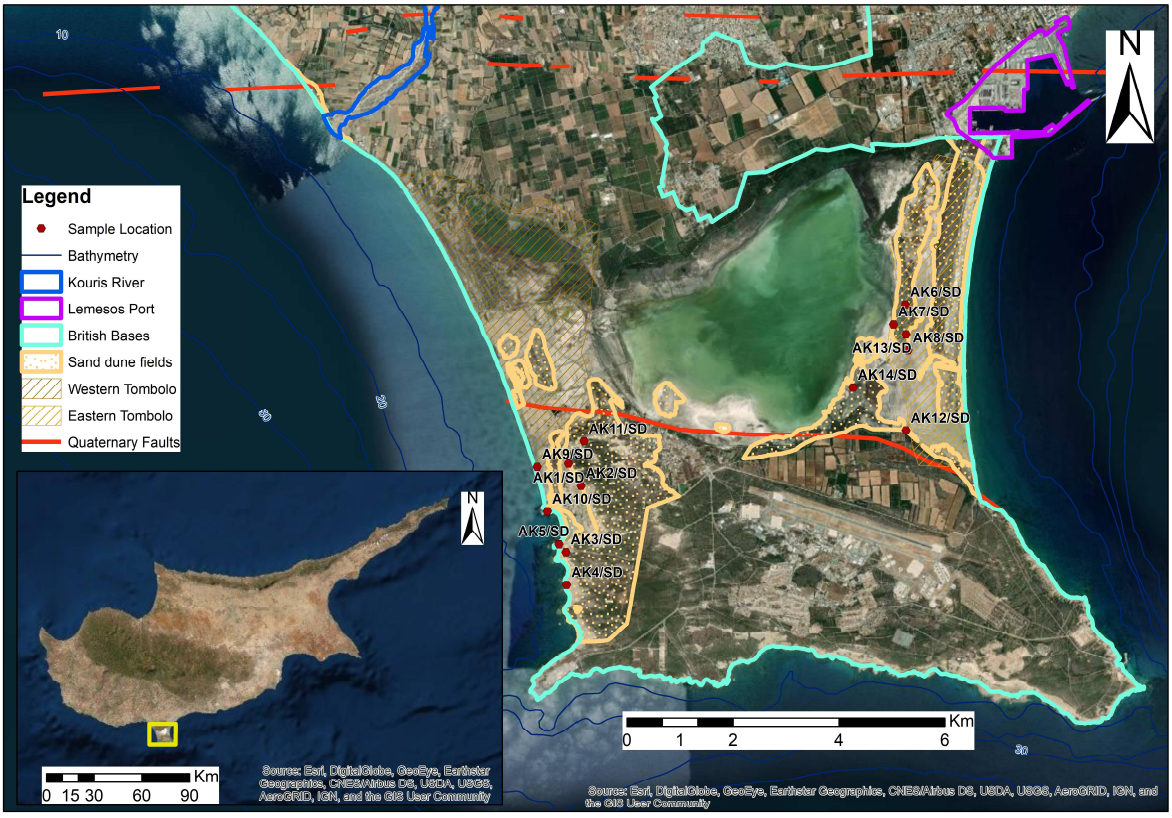


Figure 1. Location of the study area. Red circles represent sample location.

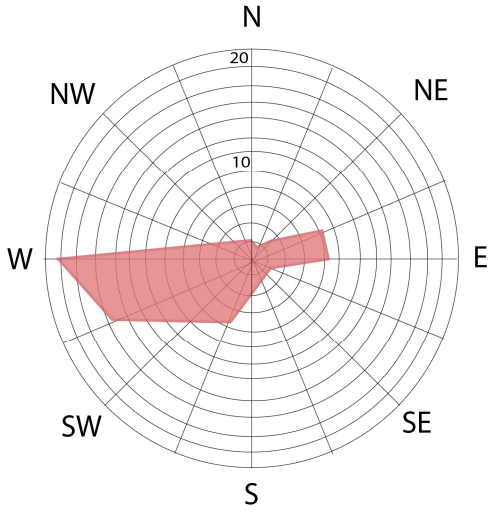


Figure 2. Main wind direction for one-year period measured at the study area. The wind rose graph shows dominant Western winds and periodical Eastern winds.

2. Material and Methods

For the evaluation of the geomorphic evolution of the study area, we conducted geomorphological mapping, remote sensing analysis, field survey and sampling (Figure 1). Fourteen sand samples were extracted from the base of dunes, both at the west and east part of the study area. Ten of the fourteen samples were qualified for further analysis (Table 1). Sampling conducted using 2 inch diameter plastic PVC tubes, which were placed horizontally against the section of the sand dune and hammered into the dune. The tubes were sealed, and the collected material remained protected from exposure to the sunlight. The samples were transported to the laboratory of "Engineering Geology and Industrial Minerals" of the Cyprus Geological Survey Department.

Table 1. Sample details.

Sample ID	Location	Type of Analysis	Distance from the Coast (m)	Elevation (m)	Humidity (%)
AK1/SD	West	Grain Size + OSL	498	1.56	0.65
AK2/SD	West	OSL	682	1.72	0.82
AK3/SD	West	Not Qualified	137	1.98	n/a
AK4/SD	West	Not Qualified	25.3	0.64	n/a
AK5/SD	West	Grain size + OSL	52.5	1.04	2.69
AK6/SD	East	OSL	1135	0.34	1.74
AK7/SD	East	Not Qualified	1331.4	0.21	n/a
AK8/SD	East	Not Qualified	1084.7	0.47	n/a
AK9/SD	West	Grain size	17.67	1.08	2.05
AK10/SD	West	Grain size	13.69	2.13	0.97
AK11/SD	West	Grain size	870	12.17	0.71
AK12/SD	East	Grain size	963.76	2.56	1.98
AK13/SD	East	Grain size	1733	0.54	0.42
AK14/SD	East	Grain size	116.85	0.57	0.56

2.1. Geochronology

Geochronological studies with optically stimulated luminescence (OSL) dating method was applied to four samples. Three samples retrieved from the western dunes and one sample from the eastern dune field. In-situ measurements for natural radioactivity of the predominating sand formations were taken by handheld scintillometers (Saphymo-Stell, model spp-2). The samples were processed and measured by the Laboratory of Palaeoenvironment and Ancient Metals Studies (PAMS lab), National Center for Scientific Research «DEMOKRITOS», Greece. All laboratory procedures were performed under controlled illumination conditions (subdued ~580 nm light) in order to extract samples' light-safe interior. The calculations of the external dose rates (U, Th, K) were based on analytical data obtained by Inductively Coupled Plasma Mass Spectrometry (ICP-MS; ACME laboratories, Canada). Water content (%) was based on modern values with an error of ±15% and considered to remain constant during burial. Chemical treatment was conducted following well established laboratory protocols and standardized procedures [20,47]. Luminescence measurements were carried out using a RISØ-TL/OSL-15 reader.

2.2. Grain Size Analysis

Sieving analysis performed to the collected samples. For the determination of grain size, 8 samples (Table 1) were analyzed and classified based on Folk's, 1954 nomenclature [48]. Samples weighting between 200 and 300 g were dried for over 24 h at temperatures 100–110 °C. They were then weighed and sieved through a set of sieves (diameter of the sieves from 10 mm to 0.053 mm, according to CYSEN 933-1:2012). The statistical parameters, used for sedimentological interpretations such as mean, sorting, skewness, and kurtosis were calculated using Gradistat V.4 software [49].

3. Results

3.1. Western Sand Dune Fields

The western dune fields are extending for approximately 6 km (north to south) and 1.6 km inland (west to east) (Figure 1). The primary dunes are located near the coastline, extending approximately until 200 m inland. They are mostly composed of loose sand, reaching heights up to a few meters and they are bare of vegetation (Figure 3). Based on the grain size analysis the western primary dunes (AK9/SD) are characterized as trimodal, very poorly sorted fine sand (Figure 4).

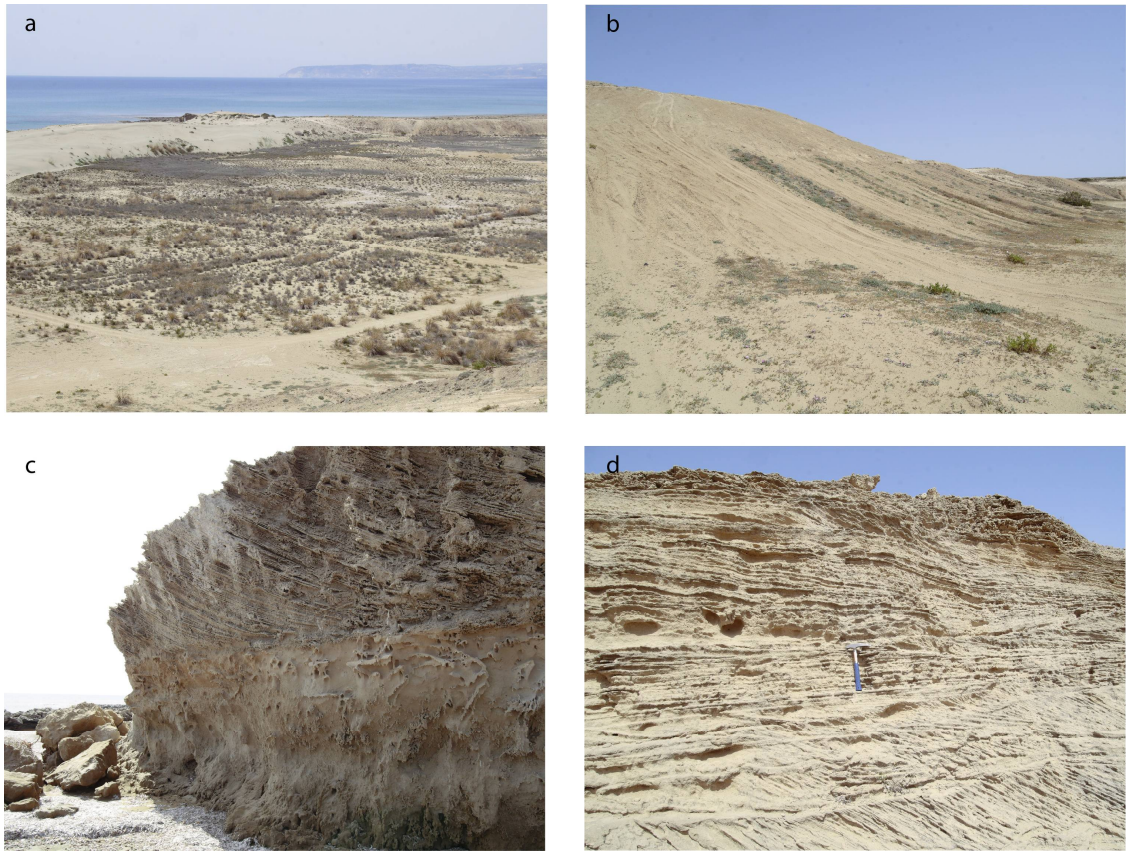


Figure 3. Western dune fields (**a**) primary dune development near the coastline. (**b**) Dune with height up to 48 m. (**c**) Lithified dune (aeolianite) near the coastline with clear evidence of erosion (weathered notch) and (**d**) Lithified with lamination.

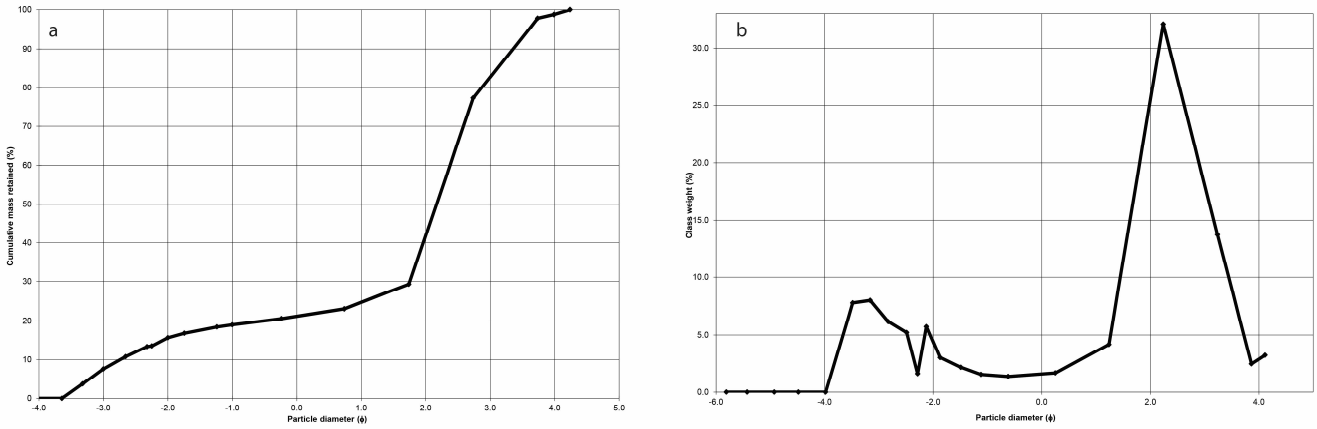


Figure 4. Cumulative (phi) and Distribution (phi) curves. (**a**,**b**) sample AK9/SD.

Semi-lithified dunes are lying behind the primary dunes. They extend approximately 470 m inland and they are covered by vegetation, contrary to the completely bare sand of the primary dunes. Their height is reaching approximately 10 m (Figure 3). After the grain size analysis, the dunes (AK5/SD and AK10/SD) are characterized as unimodal, moderately well sorted, fine sand (Figure 5).

Lithified sand dunes are following the semi-lithified dune and they are extending approximately 1.5 km inland from the coastline. They are composed of layers of sediments with plane-parallel bedding and their maximum height reaches approximately 48 m. The vegetation is denser with a variety of plant species and even small trees (Figure 3). On top of the lithified sand dunes there is very little exposed sand. After the grain size analysis, the western dunes (AK1/SD and AK11/SD) are characterized as Unimodal, Poorly Sorted, fine sand (Figure 6).

3.2. Eastern Sand Dune Fields

The eastern dune fields are extending for approximately 4.8 km and they are lying from the coastline up to 1.4 km inland (Figure 1). Primary dunes are located in close proximity to the coastline. Their height reaches up to 2 m and they consist of loose sand. There is no evidence of vegetation on top of the dunes (Figure 7). After the grain size analysis, the eastern primary dunes (AK12/SD) are characterized as trimodal, very poorly sorted, fine sand (Figure 8).

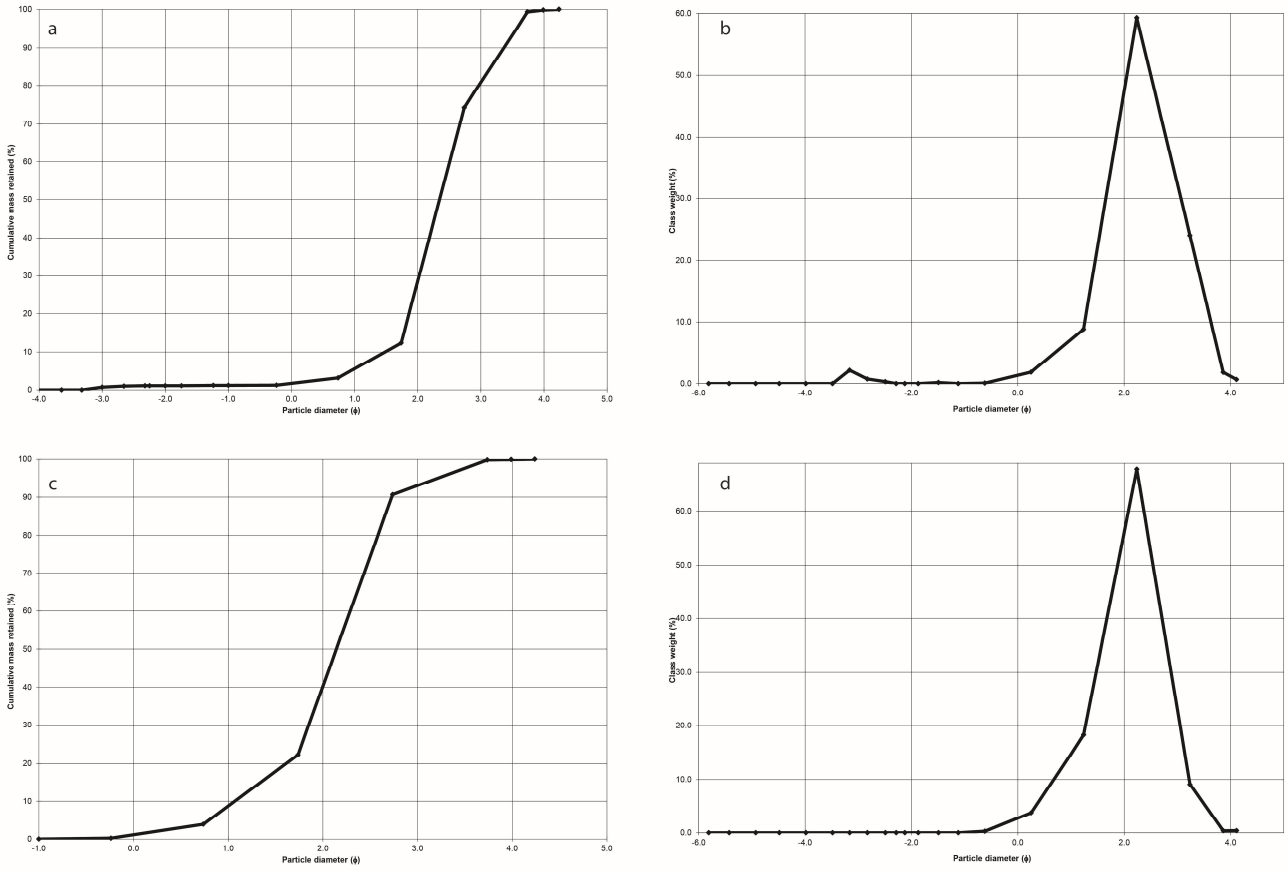


Figure 5. Cumulative (phi) and Distribution (phi) curves. (**a**,**b**) sample AK5/SD. (**c**,**d**) sample AK10/SD.

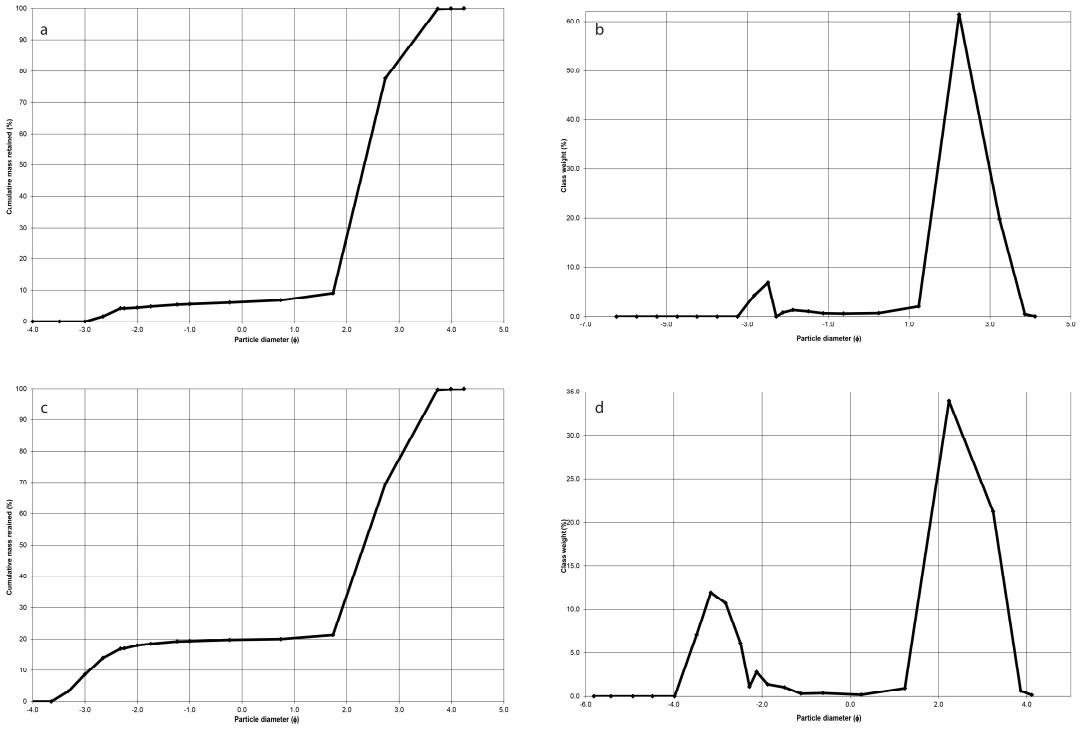


Figure 6. Cumulative (phi) and Distribution (phi) curves. (**a**,**b**) sample AK1/SD. (**c**,**d**) sample AK11/SD.



Figure 7. Eastern dune fields (**a**) coppice dunes (**b**) sampling of the coppice dunes (**c**) primary development next to the coastline, covering archeological ruins.

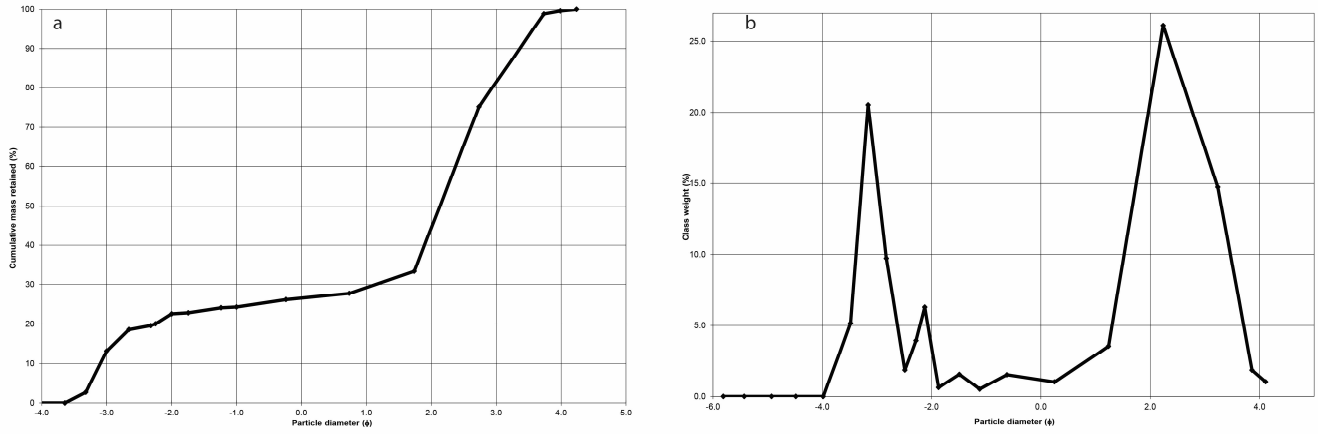


Figure 8. Cumulative (phi) and Distribution (phi) curves. (**a**,**b**) sample AK12/SD.

The primary dunes are followed by coppice dunes which considered as the initial stage of the formation of new foredunes [50] (Figure 7). Their maximum height reaches approximately 4 m. No visible layers of sedimentation were observed. After the grain size analysis, the eastern coppice dunes (AK13/SD and AK14/SD) are characterized as Unimodal, moderately well sorted, fine sand (Figure 9).

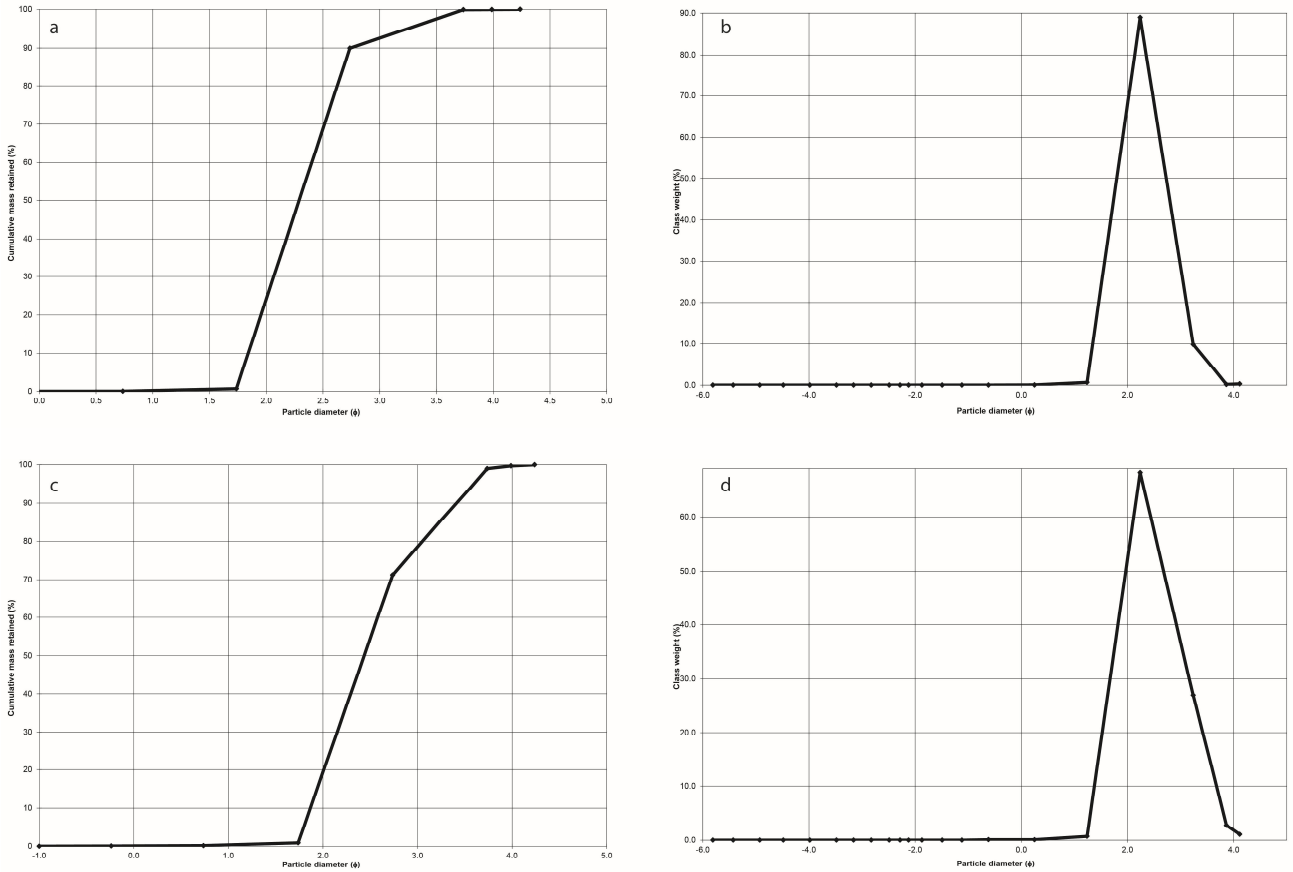


Figure 9. Cumulative (phi) and Distribution (phi) curves. (**a**,**b**) sample AK13/SD. (**c**,**d**) sample AK14/SD.

3.3. OSL Measurements

Quartz grains in the 200–250 μm fraction provided appropriate OSL signals that could be used for estimating reliable palaeodoses and thus the age of the samples.

Dose rates were calculated using the software tool "DRc" [51]. The age estimates are given with 1σ in Table 2. OSL ages were calculated based on the simplified equation shown below and using the Central Age model proposed by Galbraith et al., (1999) [52].

$$Age = \frac{Paleodose\ (Gy)}{Dose\ rate\ (Gy/ka)}$$

Table 2. Measured palaeodoses (Des), calculated total dose rates (DRs) and calculated ages derived using the OSL protocol after [20]. The grain size is 200–250 μm for all samples.

Sample ID	De (Gy)	DR (Gy/ka)	Age (ka)
AK 1/SD	23.7 ± 1.9	0.588 ± 0.04	40.3 ± 4.2
AK 2/SD	32.6 ± 2.3	0.569 ± 0.039	56.2 ± 5.5
AK 5/SD	22.0 ± 2.3	0.562 ± 0.039	39.2 ± 4.9
AK 6/SD	NO RESULT	0.520 ± 0.038	NO RESULT

4. Discussion

Climate conditions, especially wind regime seems to have a significant role for the activation, mobilization and elongation of dunes during the cold and dry periods of the late Quaternary [53–56]. When global wind power decreased during the Holocene, vegetated dune fields usually stabilized [57].

Pleistocene, high-energy fluvial material from the Kouris river catchment area, north of the western dune field, transported and deposited alluvium over the south-western part of Akrotiri peninsula which resulted the development of the western tombolo. These material is known as Fanglomerate formation [58]. These alluvial surfaces serve as a substrate over which most of the western dune field developed. Similar type of development is also know from the area of Negev in Israel, which resulted the vegetated linear dunes encroached on top of alluvial surfaces during Pleistocene [59]. According to Roskin et al., 2017 [60], It seems that during the late Pleistocene when climate fluctuations (changes in wind power, precipitation) had larger amplitudes [57,61], aeolian-fluvial interactions were more common in semi-arid environments and desert margins [62–64].

The Western dune field provided an age of 56.2 ± 5.5 ka, based on the oldest OSL sample extracted from the base of the aeolianite formation (Table 2). This age is in agreement with previous studies at the SE Cyprus, which provided ages of aeolianites approximately 65 ka [65], providing additional evidence for aeolian depositional events in SE and S Cyprus mainly after the MIS 5a. OSL ages in eastern Mediterranean aeolianites and littoral deposits have been dated as late Pleistocene, indicating that the formation of sand dunes mainly occurred in episodes in the time interval of the MIS 2, 3, 4 and 5 [65–67], showing a common late Pleistocene framework of deposition.

The material from the erosion of the western sand dunes moved along with the anticlockwise longshore drift [34] accumulated to the east side of the peninsula, in front of the already formed spit/beach ridge during Middle to Upper Holocene [31]. Beach ridges composed of shallow marine sediments downdip of lagoonal deposits are barriers. These are often associated with relative sea-level rise, thus representing a transgressive depositional complex [68]. Aeolian beach ridges are often linked to sea-level highstand [69] representing transgressive [70] or highstand deposits [71], or they are aggradational deposits formed by aeolian reworking of the transgressive beach ridge during times of relative sea-level stability [72]. On top of the flat terrain area of eastern side of Akrotiri peninsula, sand dunes were formed during the upper Holocene. The East dune field is considered to be directly connected with the regional sea level fluctuations [31] and tectonics [73] which formed the coastal landscape and with the development of the beach ridge provided the substrate for the formation of the dunes [74].

Regarding the above data, it is suggested that the area between the mainland and the former Akrotiri island was open before 56 ka (Figure 10a). The western side tombolo of Akrotiri peninsula was already formed before 56.2 ± 5.5 ka creating a bay with an opening

to the sea on the east (Figure 10b). On top of the tombolo the sand dunes started to develop and were slowly mobilized to the east. Through climatic changes and tectonic forces, the sand dunes passed through a series of erosion and accumulation phases and eventually with the loss of land due to sea level changes the dune field suffered significant erosion. The eastern dune field developed after the creation of the spit/beach ridge in Upper Holocene, due to the sea level fluctuation (Figure 10c). The formation of both dune fields assisted to the isolation of the salt lake at the center of the peninsula and played an important role to the paleogeographic development of the eastern area of the peninsula [31].

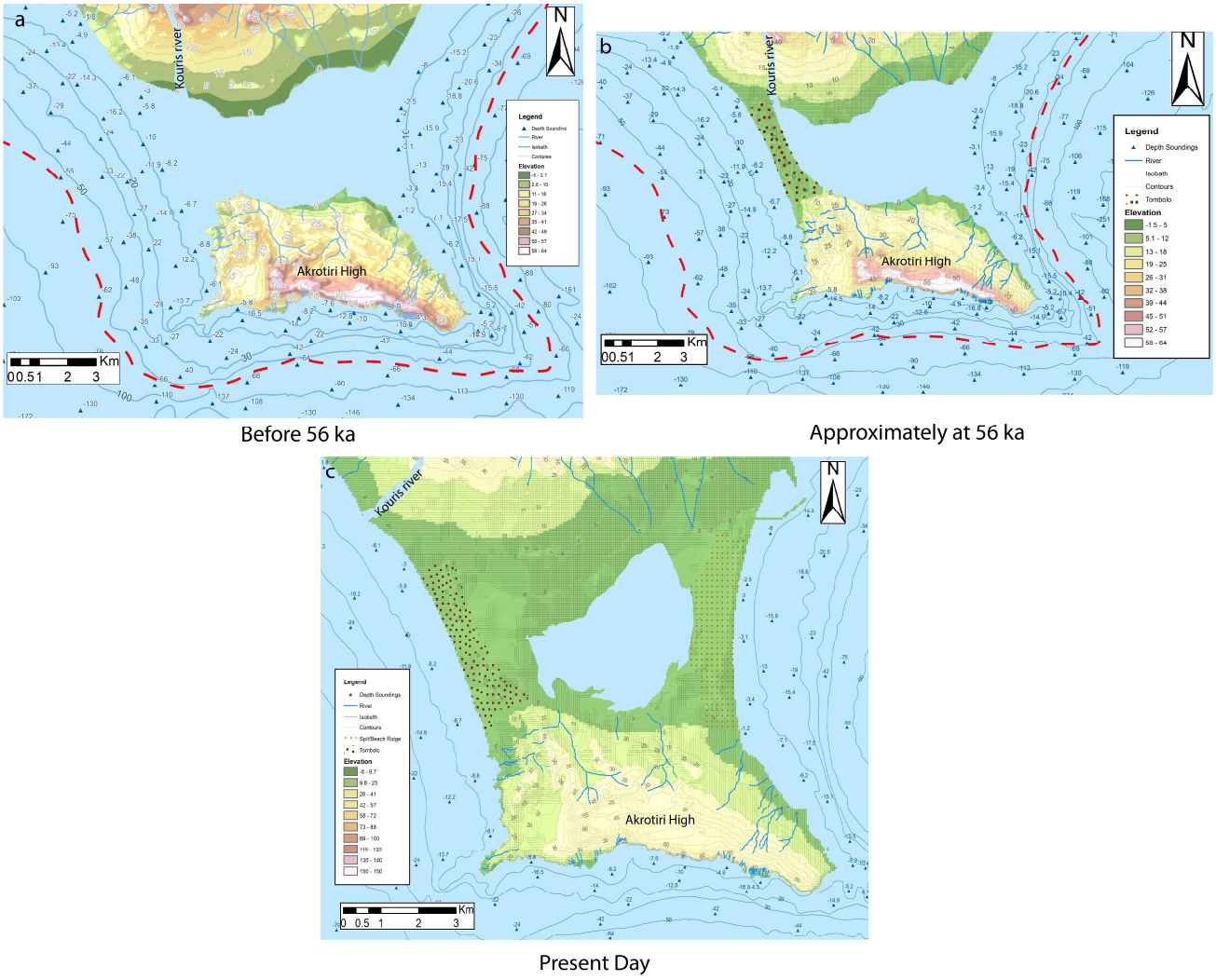


Figure 10. Palaeogeographic evolution of Akrotiri peninsula. (**a**) before 56 ka, red dashed line represent hypothetical palaeocoastline without estimation of G.I.A and tectonics of the area (**b**) at approximately 56 ka, red dashed line represent hypothetical palaeocoastline without estimation of G.I.A and tectonics of the area (**c**) present day.

5. Conclusions

The development of the sand dune fields at Akrotiri peninsula is driven by the supply of material by Kouris river to their source beaches and the movement of the material by the prevailing winds. Also, the tectonic forces from the activation of Quaternary faults and the climatic changes, resulted in the erosion of the dunes through the sea level fluctuations. At the Western side of the peninsula, there is a long record of dune development which started at approximately 56 ka BP and continued with multiple layers of deposition and periods of significant erosion. Dune development and mobilization is still under process and the prevailing western winds have contributed to the enlargement of the dune field.

At the eastern side of the peninsula, the dune field developed in a much later stage in the Upper Holocene. The chronology of the dunes yields a very recent development, which is consistent with the unconsolidated state of the sediment, the low height of the dunes and the absence of vegetation.

Our study further highlights that the morphological and geochronological analysis of sand dune fields in the eastern Mediterranean along with other geomorphological features can provide a significant tool to the paleogeographic reconstruction of an area.

Author Contributions: Conceptualization, M.P. and N.E.; Investigation, M.P.; Methodology, N.E. and M.P.; Supervision, M.P. and N.E.; Writing—original draft, M.P.; Writing—review & editing, N.E. and M.P. All authors have read and agreed to the published version of the manuscript.

Funding: This research was funded by Honor Frost Foundation, 10 Carlton House Terrace, London SW1Y 5AH, "Small Grant Award".

Data Availability Statement: Not applicable.

Acknowledgments: The authors would like to thank Honor Frost Foundation for funding and supporting the activities of this research. Also, the authors would like to thank Y. Bassiakos, E. Filippaki and E. Tsakalos of the National Center for Scientific Research «DEMOKRITOS», Greece for their support regarding the geochronological analysis of the samples. Also, the authors would like to thank the anonymous reviewers for their fruitful comments.

Conflicts of Interest: The authors declare no conflict of interest.

References

1. Tsoar, H. Geomorphology and Paleogeography of Sand Dunes That Have Formed Thekurkar Ridges in the Coastal Plain of Israel. *Isr. J. Earth Sci.* **2000**, *49*, 189–196. [CrossRef]
2. Aagaard, T.; Orford, J.; Murray, A.S. Environmental Controls on Coastal Dune Formation; Skallingen Spit, Denmark. *Geomorphology* **2007**, *83*, 29–47. [CrossRef]
3. Costas, S.; Jerez, S.; Trigo, R.M.; Goble, R.; Rebêlo, L. Sand Invasion along the Portuguese Coast Forced by Westerly Shifts during Cold Climate Events. *Quat. Sci. Rev.* **2012**, *42*, 15–28. [CrossRef]
4. Costas, S.; Naughton, F.; Goble, R.; Renssen, H. Windiness Spells in SW Europe since the Last Glacial Maximum. *Earth Planet. Sci. Lett.* **2016**, *436*, 82–92. [CrossRef]
5. Delgado-Fernandez, I.; Davidson-Arnott, R. Meso-Scale Aeolian Sediment Input to Coastal Dunes: The Nature of Aeolian Transport Events. *Geomorphology* **2011**, *126*, 217–232. [CrossRef]
6. Hesp, P.A.; Walker, I.J. Coastal dunes. In *Treatise on Geomorphology*; Elsevier Inc.: Amsterdam, The Netherlands, 2013; Volume 11, pp. 328–355. [CrossRef]
7. Psuty, N.P.; Silveira, T.M. Global Climate Change: An Opportunity for Coastal Dunes? *J. Coast. Conserv.* **2010**, *14*, 153–160. [CrossRef]
8. Pye, K. Coastal Dunes. *Prog. Phys. Geogr. Earth Environ.* **1983**, *7*, 531–557. [CrossRef]
9. Feagin, R.A.; Sherman, D.J.; Grant, W.E. Coastal Erosion, Global Sea-Level Rise, and the Loss of Sand Dune Plant Habitats. *Front. Ecol. Environ.* **2005**, *3*, 359–364. [CrossRef]
10. Miller, T.E.; Gornish, E.S.; Buckley, H.L. Climate and Coastal Dune Vegetation: Disturbance, Recovery, and Succession. *Plant. Ecol.* **2010**, *206*, 97–104. [CrossRef]
11. Davidson-Arnott, R.; Law, M. Measurement and Prediction of Long-Term Sediment Supply to Coastal Foredunes. *J. Coast. Res.* **1996**, *12*, 654–663.
12. Pye, K.; Blott, S.J. Evolution of a Sediment-Starved, over-Stabilised Dunefield: Kenfig Burrows, South Wales, UK. *J. Coast. Conserv.* **2017**, *21*, 685–717. [CrossRef]
13. Shanahan, C.; Montoya, B.M. Erosion Reduction of Coastal Sands Using Microbial Induced Calcite Precipitation. *Geo-Chicago* **2016**, *2016*, 42–51. [CrossRef]
14. Roelvink, D.; Reniers, A.; van Dongeren, A.; van Thiel de Vries, J.; McCall, R.; Lescinski, J. Modelling Storm Impacts on Beaches, Dunes and Barrier Islands. *Coast. Eng.* **2009**, *56*, 1133–1152. [CrossRef]
15. Hallermeier, R.J.; Rhodes, P.E. Generic Treatment of Dune Erosion for 100-Year Event. *Coast. Eng.* **1989**, *1988*, 1197–1211. [CrossRef]
16. Sherman, D.J.; Jackson, D.W.T.; Namikas, S.L.; Wang, J. Wind-Blown Sand on Beaches: An Evaluation of Models. *Geomorphology* **1998**, *22*, 113–133. [CrossRef]
17. Sherman, D.J. Understanding Wind-Blown Sand: Six Vexations. *Geomorphology* **2020**, *366*, 107193. [CrossRef]
18. Hoffmann, G.; Lampe, R.; Barnasch, J. Postglacial Evolution of Coastal Barriers along the West Pomeranian Coast, NE Germany. *Quat. Int.* **2005**, *133–134* (Suppl. 1), 47–59. [CrossRef]

19. Reimann, T.; Tsukamoto, S.; Harff, J.; Osadczuk, K.; Frechen, M. Reconstruction of Holocene Coastal Foredune Progradation Using Luminescence Dating—An Example from the Świna Barrier (Southern Baltic Sea, NW Poland). *Geomorphology* **2011**, *132*, 1–16. [CrossRef]
20. Murray, A.S.; Wintle, A.G. Luminescence Dating of Quartz Using an Improved Single-Aliquot Regenerative-Dose Protocol. *Radiat. Meas.* **2000**, *32*, 57–73. [CrossRef]
21. Cordier, S. Optically Stimulated Luminescence Dating: Procedures and Applications to Geomorphological Research in France. *Geomorphologie* **2010**, *16*, 21–40. [CrossRef]
22. Del Valle, L.; Pomar, F.; Fornós, J.J.; Gómez-Pujol, L.; Timar-Gabor, A. Lower to Middle Pleistocene Coastal Dune Fields Formation in the Western Mediterranean (Western Eivissa, Balearic Archipelago): Chronology and Landscape Evolution. *Aeolian Res.* **2020**, *45*, 100595. [CrossRef]
23. He, Z.; Zhou, J.; Lai, Z.P.; Yang, L.H.; Liang, J.M.; Long, H.; Ou, X.J. Quartz OSL Dating of Sand Dunes of Late Pleistocene in the Mu Us Desert in Northern China. *Quat. Geochronol.* **2010**, *5*, 102–106. [CrossRef]
24. Peng, J.; Dong, Z.; Han, F. Optically Stimulated Luminescence Dating of Sandy Deposits from Gulang County at the Southern Margin of the Tengger Desert, China. *J. Arid Land* **2016**, *8*, 1–12. [CrossRef]
25. Ning, W.X.; Wang, Z.T. Pattern Analysis and Dating for the Badain Jaran Dune Field, Northwestern China. *Environ. Earth Sci.* **2020**, *79*, 1–11. [CrossRef]
26. Hadjichambis, A.C.; Paraskeva-Hadjichambi, D.; Dimopoulos, P.; Hadjichambis, A.C.; Della, A.; Paraskeva-Hadjichambi, D.; Georghiou, K.; Dimopoulos, P. Flora of the Sand Dune Ecosystems of Cyprus European Network for Environmental Citizenship View Project Vegetation of Europe View Project Flora of the Sand Dune Ecosystems of Cyprus. 2004. Available online: https://www.semanticscholar.org/paper/Flora-of-the-sand-dune-ecosystems-of-Cyprus-Hadjichambis-Della/53d46e610c2b5ccecb3920e8cd846c210c884af4 (accessed on 29 October 2021).
27. Della, A.; Iatrou, G. New Plant Records from Cyprus. *Kew Bull.* **1996**, *50*, 387–396. [CrossRef]
28. Loizides, M.; Carbone, M.; Alvarado, P. Geoglossum Dunense (Ascomycota, Geoglossales): A New Species from the Mediterranean Islands of Cyprus and Malta. *Mycol. Prog.* **2015**, *14*, 1–8. [CrossRef]
29. Zomeni, Z. Quaternary Marine Terraces on Cyprus: Constraints on Uplift and Pedogenesis, and the Geoarchaeology of Palaipafos. Ph.D. Thesis, Oregon State University, Corvallis, OR, USA, 2012.
30. Polidorou, M.; Saitis, G.; Evelpidou, N. Beachrock Development as an Indicator of Paleogeographic Evolution, the Case of Akrotiri Peninsula, Cyprus. *Z. Geomorphol.* **2021**, 3–17. [CrossRef]
31. Polidorou, M.; Evelpidou, N.; Tsourou, T.; Drinia, H.; Salomon, F.; Blue, L. Observations on Palaeogeographical Evolution of Akrotiri Salt Lake, Lemesos, Cyprus. *Geosciences* **2021**, *11*, 321. [CrossRef]
32. Milnes, E. Process-Based Groundwater Salinisation Risk Assessment Methodology: Application to the Akrotiri Aquifer (Southern Cyprus). *J. Hydrol.* **2011**, *399*, 29–47. [CrossRef]
33. Bear, L.; Morel, S. *The Geology and Mineral Resources of the Agros-Akrotiri Area*; Cyprus Geological Survey Department: Nicosia, Cyprus, 1960.
34. Garzanti, E.; Andò, S.; Scutellà, M. Actualistic Ophiolite Provenance: The Cyprus Case. *J. Geol.* **2000**, *108*, 199–218. [CrossRef]
35. Zavatarielli, M.; Mellor, L.G. A Numerical Study of the Mediterranean Sea Circulation. *J. Phys. Oceanogr.* **1995**, *25*, 1384–1414. [CrossRef]
36. Saaroni, H.; Halfon, N.; Ziv, B.; Alpert, P.; Kutiel, H. Links between the Rainfall Regime in Israel and Location and Intensity of Cyprus Lows. *Int. J. Climatol.* **2010**, *30*, 1014–1025. [CrossRef]
37. Rojas, R.; Feyen, L.; Watkiss, P. Climate Change and River Floods in the European Union: Socio-Economic Consequences and the Costs and Benefits of Adaptation. *Glob. Environ. Chang.* **2013**, *23*, 1737–1751. [CrossRef]
38. Zodiatis, G.; Drakopoulos, P.; Brenner, S.; Groom, S. Variability of the Cyprus Warm Core Eddy during the CYCLOPS Project. *Deep Sea Res. Part II Top. Stud. Oceanogr.* **2005**, *52*, 2897–2910. [CrossRef]
39. Menna, M.; Poulain, P.M.; Zodiatis, G.; Gertman, I. On the Surface Circulation of the Levantine Sub-Basin Derived from Lagrangian Drifters and Satellite Altimetry Data. *Deep Sea Res. Part I Oceanogr. Res. Pap.* **2012**, *65*, 46–58. [CrossRef]
40. Goldsmith, V.; Rosen, P.; Gertner, Y. Eolian transport measurements, winds, and comparison with theoretical transport in Israeli coastal dunes. In *Coastal Dunes. Form and Process*; Wiley: Chichester, UK, 1990.
41. Tsoar, H. Trends in the Development of Sand Dunes along the Southeastern Mediterranean Coast in Dunes of the European Coasts. Geomorphology–Hydrology–Soils. *Catena. Suppl.* **1990**, *18*, 51–60.
42. Tsoar, H.; Blumberg, D.G. Formation of Parabolic Dunes from Barchan and Transverse Dunes along Israel's Mediterranean Coast. *Earth Surf. Process. Landforms* **2002**, *27*, 1147–1161. [CrossRef]
43. Tsoar, H. Sand Dunes Mobility and Stability in Relation to Climate. *Phys. A Stat. Mech. Its Appl.* **2005**, *357*, 50–56. [CrossRef]
44. Schilman, B.; Bar-Matthews, M.; Almogi-Labin, A.; Luz, B. Global Climate Instability Reflected by Eastern Mediterranean Marine Records during the Late Holocene. *Palaeogeogr. Palaeoclimatol. Palaeoecol.* **2001**, *176*, 157–176. [CrossRef]
45. Indermühle, A.; Stocker, T.F.; Joos, F.; Fischer, H.; Smith, H.J.; Wahlen, M.; Deck, B.; Mastroianni, D.; Tschumi, J.; Blunier, T.; et al. Holocene Carbon-Cycle Dynamics Based on CO_2 Trapped in Ice at Taylor Dome, Antarctica. *Nature* **1999**, *398*, 121–126. [CrossRef]
46. Lückge, A.; Doose-Rolinski, H.; Khan, A.A.; Schulz, H.; Von Rad, U. Monsoonal Variability in the Northeastern Arabian Sea during the Past 5000 Years: Geochemical Evidence from Laminated Sediments. *Palaeogeogr. Palaeoclimatol. Palaeoecol.* **2001**, *167*, 273–286. [CrossRef]

47. Preusser, F.; Degering, D.; Fuchs, M.; Hilgers, A.; Kadereit, A.; Klasen, N.; Krbetschek, M.; Richter, D.; Spencer, J.Q.G. Luminescence Dating: Basics, Methods and Applications. *E G Quat. Sci. J.* **2008**, *57*, 95–149. [CrossRef]
48. Folk, R.L. The Distinction between Grain Size and Mineral Composition in Sedimentary-Rock Nomenclature. *J. Geol.* **1954**, *62*, 344–359. [CrossRef]
49. Blott, S.J.; Pye, K. GRADISTAT: A Grain Size Distribution and Statistics Package for the Analysis of Unconsolidated Sediments. *Earth Surf. Process. Landforms* **2001**, *26*, 1237–1248. [CrossRef]
50. El Banna, M.M. Nature and Human Impact on Nile Delta Coastal Sand Dunes, Egypt. *Environ. Geol.* **2003**, *45*, 690–695. [CrossRef]
51. Tsakalos, E.; Christodoulakis, J.; Charalambous, L. The Dose Rate Calculator (DRc) for Luminescence and ESR Dating-a Java Application for Dose Rate and Age Determination. *Archaeometry* **2016**, *58*, 347–352. [CrossRef]
52. Galbraith, R.F.; Roberts, R.G.; Laslett, G.M.; Yoshida, H.; Olley, J.M. Optical Dating of Single and Multiple Grains of Quartz from Jinmium Rock Shelter, Northern Australia: Part I, Experimental Design and Statistical Models. *Archaeometry* **1999**, *41*, 339–364. [CrossRef]
53. Stone, A.E.C.; Thomas, D.S.G. Linear Dune Accumulation Chronologies from the Southwest Kalahari, Namibia: Challenges of Reconstructing Late Quaternary Palaeoenvironments from Aeolian Landforms. *Quat. Sci. Rev.* **2008**, *27*, 1667–1681. [CrossRef]
54. Telfer, M.W.; Bailey, R.M.; Burrough, S.L.; Stone, A.E.S.; Thomas, D.S.G.; Wiggs, G.S.F. Understanding Linear Dune Chronologies: Insights from a Simple Accumulation Model. *Geomorphology* **2010**, *120*, 195–208. [CrossRef]
55. Roskin, J.; Tsoar, H.; Porat, N.; Blumberg, D.G. Palaeoclimate Interpretations of Late Pleistocene Vegetated Linear Dune Mobilization Episodes: Evidence from the Northwestern Negev Dunefield, Israel. *Quat. Sci. Rev.* **2011**, *30*, 3364–3380. [CrossRef]
56. Thomas, D.S.G.; Bailey, R.M. Is There Evidence for Global-Scale Forcing of Southern Hemisphere Quaternary Desert Dune Accumulation? A Quantitative Method for Testing Hypotheses of Dune System Development. *Earth Surf. Process. Landforms* **2017**, *42*, 2280–2294. [CrossRef]
57. Mcgee, D.; Broecker, W.S.; Winckler, G. Gustiness: The Driver of Glacial Dustiness? *Quat. Sci. Rev.* **2010**. [CrossRef]
58. Poole, A.; Robertson, A. Pleistocene Fanglomerate Deposition Related to Uplift of the Troodos Ophiolite, Cyprus. *Proc. Ocean Drill. Progr. Sci. Results* **1998**, *160*, 545–568. [CrossRef]
59. Roskin, J.; Katra, I.; Porat, N.; Zilberman, E. Evolution of Middle to Late Pleistocene Sandy Calcareous Paleosols Underlying the Northwestern Negev Desert Dunefield (Israel). *Palaeogeogr. Palaeoclimatol. Palaeoecol.* **2013**, *387*, 134–152. [CrossRef]
60. Roskin, J.; Bookman, R.; Friesem, D.E.; Vardi, J. A Late Pleistocene Linear Dune Dam Record of Aeolian-Fluvial Dynamics at the Fringes of the Northwestern Negev Dunefield. *Sediment. Geol.* **2017**, *353*, 76–95. [CrossRef]
61. Vaks, A.; Bar-Matthews, M.; Ayalon, A.; Matthews, A.; Frumkin, A.; Dayan, U.; Halicz, L.; Almogi-Labin, A.; Schilman, B. Paleoclimate and Location of the Border between Mediterranean Climate Region and the Saharo–Arabian Desert as Revealed by Speleothems from the Northern Negev Desert, Israel. *Earth Planet. Sci. Lett.* **2006**, *249*, 384–399. [CrossRef]
62. Liu, B.; Coulthard, T.J. Mapping the Interactions between Rivers and Sand Dunes: Implications for Fluvial and Aeolian Geomorphology. *Geomorphology* **2015**, *231*, 246–257. [CrossRef]
63. Robins, L.; Greenbaum, N.; Yu, L.P.; Bookman, R.; Roskin, J. High-Resolution Portable-OSL Analysis of Vegetated Linear Dune Construction in the Margins of the Northwestern Negev Dunefield (Israel) during the Late Quaternary. *Aeolian Res.* **2021**, *50*, 100680. [CrossRef]
64. Robins, L.; Roskin, J.; Yu, L.; Greenbaum, N. Aeolian-Fluvial Sediments and Landscapes along the Northwestern Negev Dunefield (Israel) Margins since the Late Pleistocene. In Proceedings of the 23rd EGU General Assembly, Online, 19–30 April 2021.
65. Tsakalos, E. Geochronology and Exoscopy of Quartz Grains in Environmental Determination of Coastal Sand Dunes in SE Cyprus. *J. Archaeol. Sci. Rep.* **2016**, *7*, 679–686. [CrossRef]
66. Athanassas, C.; Zacharias, N. Recuperated-OSL Dating of Quartz from Aegean (South Greece) Raised Pleistocene Marine Sediments: Current Results. *Quat. Geochronol.* **2010**, *5*, 65–75. [CrossRef]
67. Elmejdoub, N.; Mauz, B.; Jedoui, Y. Sea-Level and Climatic Controls on Late Pleistocene Coastal Aeolianites in the Cap Bon Peninsula, Northeastern Tunisia. *Boreas* **2011**, *40*, 198–207. [CrossRef]
68. Mellett, C.L.; Hodgson, D.M.; Lang, A.; Mauz, B.; Selby, I.; Plater, A.J. Preservation of a Drowned Gravel Barrier Complex: A Landscape Evolution Study from the North-Eastern English Channel. *Mar. Geol.* **2012**, *315–318*, 115–131. [CrossRef]
69. Brooke, B. The Distribution of Carbonate Eolianite. *Earth Sci. Rev.* **2001**, *55*, 135–164. [CrossRef]
70. Thom, B.G.; Bowman, G.M.; Roy, P.S. Late Quaternary Evolution of Coastal Sand Barriers, Port Stephens-Myall Lakes Area, Central New South Wales, Australia. *Quat. Res.* **1981**, *15*, 345–364. [CrossRef]
71. Murray-Wallace, C.V.; Bourman, R.P.; Prescott, J.R.; Williams, F.; Price, D.M.; Belperio, A.P. Aminostratigraphy and Thermoluminescence Dating of Coastal Aeolianites and the Later Quaternary History of a Failed Delta: The River Murray Mouth Region, South Australia. *Quat. Geochronol.* **2010**, *5*, 28–49. [CrossRef]
72. Hearty, P.J.; O'Leary, M.J. Carbonate Eolianites, Quartz Sands, and Quaternary Sea-Level Cycles, Western Australia: A Chronostratigraphic Approach. *Quat. Geochronol.* **2008**, *3*, 26–55. [CrossRef]
73. Soulas, J.P. *Active Tectonics Studies in Cyprus for Seismic Risk Mitigation: The Greater Limassol Area*; Cyprus Geological Survey Department: Nicosia, Cyprus, 1999.
74. Mauz, B.; Hijma, M.P.; Amorosi, A.; Porat, N.; Galili, E.; Bloemendal, J. Aeolian Beach Ridges and Their Significance for Climate and Sea Level: Concept and Insight from the Levant Coast (East Mediterranean). *Earth Sci. Rev.* **2013**, *121*, 31–54. [CrossRef]